

ASSESSING MULTIPATH INDUCED ERRORS IN VOR SYSTEMS USING RAY-TRACING TECHNIQUES IN COMBINATION WITH DETAILED TERRAIN DATABASES

F.P. Fontan(1), D. Marote(1), A. Mayo(1), B. Sanmartin(1),
A. Castro(1) and J.J. Navarro(2)

(1)ETS Ingenieros de Telecomunicación, Campus universitario.
University of Vigo. 36200 Vigo. Spain. ffontan@tsc.uvigo.es

(2)AENA (Aeropuertos Españoles y Navegación Aérea). Division de
Navegación y Vigilancia
Josefa Varcancel 30. 280027 Madrid. Spain. jnavarro@aena.es

ABSTRACT

This paper presents a modeling tool for reproducing the propagation conditions suffered by the transmitted signal from VOR stations on its way toward a receiver fitted in an aircraft. Ground reflections and diffractions give rise to interference effects with the direct signal that can lead the VOR navigation receiver to produce erroneous bearing readings. This tool should be able to help identify the causes of errors (sources of multipath) detected during test flight. Moreover, the tool could be used when planning the siting of new VOR stations.

1. INTRODUCTION

VOR systems, although very mature and simple navigation aids, continue to be used extensively throughout the world. Existing VORs or new ones planned for installation are/will be affected by multipath from multiple sources, i.e., terrain, buildings, wind turbines, etc. In this paper, a technique based on the combined use of Uniform Theory of Diffraction (UTD) and Ray-Tracing (RT) on detailed Terrain Data Bases (TDB) is presented.

At the University of Vigo (UVIGO), under the sponsorship of AENA, Spain's Air Traffic Service provider, an existing software tool is being adapted to the specific signal propagation conditions of VOR systems using the above techniques. The tool has already been used in a number of studies: aircraft-originated multipath, satellite-to-indoor at L-Band or in-cabin propagation at cellular and WLAN bands. Some recent references are [1][2][3].

The UVIGO tool module for VOR environments can analyze extended geographic areas around the navigation aid location with sizes on the order of 100x100 km². In addition to the direct signal, the contributions taken into consideration by the UVIGO tool are single, double and triple reflections, and single and double diffractions. Additionally, mixed rays encompassing reflections and diffractions can also taken into consideration. Further improvements are expected to be developed in the framework of the existing collaboration agreement including (1) in-detail analysis of Doppler-VOR antennas and (2) the scattering characteristics of large man-made objects found in the vicinity of VOR sites such as wind turbines.

The tool will also interface a VOR transmit-receive chain simulator so that propagation results can be readily translated into path deviation errors (in degrees). This will allow results obtained with this tool to be validated through comparisons with test flight measurements.

Preliminary comparisons between measurements and simulations will also be presented. During the course of the work it is expected that a full validation of the tool with actual airborne measurements will be carried out.

This tool is expected to be useful in the analysis of new VOR sittings as well as in the analysis of already existing VORs where anomalous direction readings have been reported.

2. SIMULATION TOOL BASICS

The modeling approach followed within UVIGO's propagation channel simulator is a deterministic one. This allows using detailed databases of the propagation environment. The main advantage of this approach is that it allows the identification of the various propagation mechanisms involved which are described in terms of their magnitudes, phases, delays and angles of arrival/departure (AoA/AoD).

The main steps the simulator goes through are

- ray-tracing,
- polarization-tracking,
- electromagnetic modeling, i.e., UTD,
- generation of results and

- simulation of bearing errors (transmit-receive VOR chain).

The propagation environment is described in terms of flat facets of different sizes. Environmental data for a number of cities, airports, single buildings, airplanes, etc. can be found in standard CAD/virtual reality file formats such as DXF, IGS, VRML, etc. In other cases, CAD modeling tools (e.g. AutoCAD) can be used to generate, in a convenient way, computer descriptions of the modeling scenarios to be studied.

Environment modeling does not only include geometrical aspects: material characterization for each facet in the environment files must be described from an electromagnetic point of view by means of its constants: ϵ , μ , σ . Additionally, the roughness of each facet must be included. The roughness parameter is defined as the ratio of the terrain's standard deviation with respect to the actual facet and the wavelength, $\sigma h/\lambda$. Normally, this information is not available and approximate values must be used. Figure 1 shows the correction factor due to terrain roughness for different incidence angle and $\sigma h/\lambda$ values [4]. The theoretical reflection coefficient (Figure 2) must be multiplied by this correction factor to adequately model the magnitude of reflected rays.

The tool relies on AutoCAD to handle large terrain databases. AutoCAD is also used for visualizing the rays traced with the propagation tool. From standard CAD files (.DXF) a format translation is carried out into the tool's internal format.

After this, ray-tracing and polarization-tracking techniques are used to find what possible multipath contributions are present at the receive antenna.

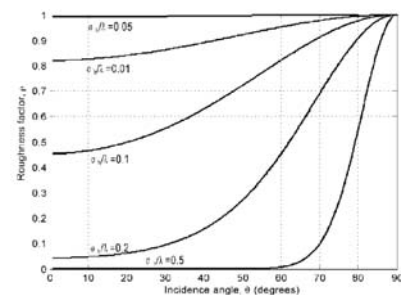


Figure 1. Correction factor due to terrain roughness.

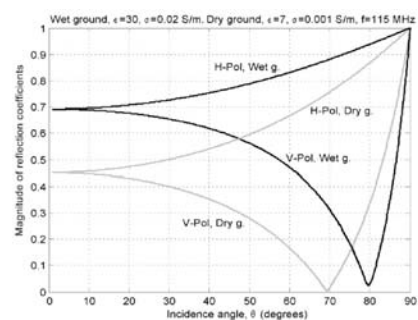


Figure 2. Vertical and horizontal reflection coefficient magnitudes for dry and wet ground.

The EM approach used is based on UGTD (Uniform Geometrical Theory of Diffraction) [5][6][7] techniques applied to the plates and wedges with flat facets and straight edges contained in the scenario database.

For such scenarios it is possible to identify three basic types of rays in addition to the direct ray (Dir):

- reflected rays (R),
- diffracted rays (D) and
- transmitted rays (T).

Transmissions are not relevant in this case but are of fundamental importance in, for instance, outdoor-to-indoor scenarios.

Further to these basic ray types, multiple rays can also be traced: double, triple, ... reflections, diffractions and transmissions. Also multiple combined (mixed) rays can be traced, e.g., RD, DR, RDR, TR, TRR, ...

Before going on to the actual electromagnetic modeling stage, a polarization-tracking study has to be performed. For each interaction, local coordinate systems must be identified to define both the parallel (\parallel) and perpendicular (\perp) vectors starting off from the transmit antenna polarization vector (in general circularly polarized, although in this particular case (VOR) the transmitted wave is horizontally polarized), i.e., its \hat{e} and $\hat{\phi}$ components, and proceed through the various interactions up to the receive antenna where, in general, elliptically polarized contributions will arrive. In the VOR case, both horizontal and vertical or, more specifically, and polarized components are received. The received \hat{e} components (XPOL) are disregarded and the co-polar ones (CPOL), $\hat{\phi}$, are kept and weighed according to the antenna received pattern. The actual EM modeling stage is then carried out. The general representation of a ray is given in the equation,

$$\vec{E}_{R,D,T} = \vec{E}(p) e^{j\phi(p)} C A(\tilde{n}_1, \tilde{n}_2, s) e^{-jk_s} \quad (1)$$

where

$E(p) e^{j\phi(p)}$ is the complex incident field, module and phase, on interaction point p ,
 C is a coefficient representing the type of interaction: reflection, diffraction, transmission,
 $A(\tilde{n}_1, \tilde{n}_2, s)$ is an amplitude or spreading factor which takes into account the geometry of the surface or edge and the type of incident ray through curvature parameters, \tilde{U} .
 e^{-jk_s} is a phase term due to the traveled propagation distance, s , from p to the receiver.

This EM modeling step provides information on the amplitudes and phases for both polarizations for the rays traced in the previous steps, where information on delay and angle of arrival/departure was already calculated.

The propagation simulation tool presents the flow diagram shown in Figure 3 where the various model elements and steps are linked together. Finally, the results module carries out some simple calculations such as receive antenna spatial filtering, receive antenna polarization loss calculations, etc. to produce the wanted results. The row results are, in principle, structured as a sequence of so-called scattering matrices made up of delta functions, two for each traced contributions (CPOL, co-polar, and XPOL, cross-polar) including information of amplitude, phase, delay and angle of arrival. Each sequence point corresponds to one sampling point along the aircraft's flight path.

The simulation tool, thus, requires a sequencing module capable of defining transmitter / receiver sampling points: aircraft flight patterns including orbits about the VOR or radial flights.

Further processing of the results file can be performed to produce more refined results suited for the current application. In the case of VOR systems, propagation results are passed on to a VOR transmit-receive chain so that actual bearing errors (in degrees) can be computed.

The radio channel created by multipath can be modeled as a linear filter whose characteristics are time-varying. The relation between the inputs and outputs of this filter may be described in the time and/or frequency domains. This means that several channel functions are possible.

The impulse response, $h(\hat{\delta})$, is one of these functions; it provides an indication of the distribution of the received echoes, their magnitudes, phases and delays. By the simple fact that the receiver is moving, the path lengths change and consequently, $h(\hat{\delta})$ is time-variant, i.e., $h(\hat{\delta}, t)$, or equivalently, space-variant: $h(\hat{\delta}, x)$. This function is given by

$$h(\hat{\delta}, x) = \sum a_{ic}(x) \tilde{a}(\hat{\delta} - \hat{\delta}_i(x)) + \sum a_{ix}(x) \tilde{a}(\hat{\delta} - \hat{\delta}_i(x)) \quad (2)$$

where

- x is the location of the receiver,
- $a_{ic}(x)$ is the complex voltage received on the co-polar field component at location x ,
- $a_{ix}(x)$ is the complex voltage received on the cross-polar field component at location x ,
- $\hat{\delta}_i(x)$ is the excess delay (relative to the direct ray) of ray i at location x .

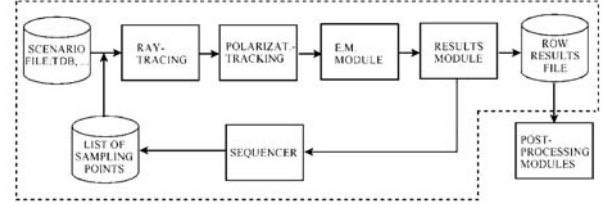


Figure 3. Block diagram of the ray-tracing tool.

An example of the impulse response is shown in Figure 4 where the co-polar contributions are shown with a circle and the cross-polar are shown with a square. A color code is used to differentiate the different ray types. Other channel function is the so-called scattering function or scattering matrix (actual sequence of row results), which shows the received echoes classified in terms of delays and Doppler shifts or equivalently, in angles of arrival, i.e.,

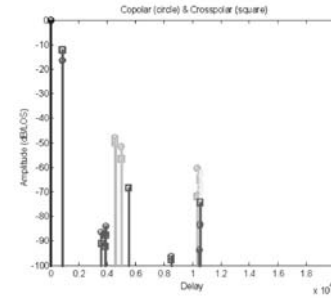


Figure 4. Example of impulse response.

$$S(\hat{\delta}, i) = \sum a_{ic}(x) \tilde{a}(\hat{\delta} - \hat{\delta}_i(x)) \tilde{a}(i - i_i(x)) + \sum a_{ix}(x) \tilde{a}(\hat{\delta} - \hat{\delta}_i(x)) \tilde{a}(i - i_i(x)) \quad (3)$$

where ν is the Doppler shift. Another system function is the channel's time/space-varying frequency response given by

$$T(t, f) = \sum_{i=0}^N a_i \exp(-j\hat{\nu}_i \hat{\delta}_i(t)) = \sum_{i=0}^N a_i \exp\left(-j \frac{2\partial}{\partial t} l_i(t)\right) \quad (4)$$

which is valid for wide-band systems and where l_i is the excess path of ray i with respect to the direct ray. This function can be particularized for a narrow-band system operating at a carrier frequency f_c and, thus, providing the actual complex envelope fading time-series,

$$r(t) = T(t, f_c) = \sum_{i=0}^N a_i \exp(-j\hat{\nu}_i \hat{\delta}_i(t)) = \sum_{i=0}^N a_i \exp\left(-j \frac{2\partial}{\partial t} l_i(t)\right) \quad (5)$$

The problem with this technique is that an extremely large number of simulation points along the aircraft route is needed. Using large terrain databases requires very long simulation times if a brute force or exhaustive search approach for locating reflection, diffraction, etc. points is used.

The UVIGO propagation tool uses an acceleration technique based on the concept of "bounding boxes". The terrain database is first split into volumetric units (bounding boxes), each encompassing a large number of terrain facets. These boxes are limited by the highest and lowest terrain points contained in it. Ray-tracing checks are thus carried out by first verifying whether a given ray goes through each box. If this is the case, the tracing module searches within that box for reflections, obstructions, etc. If this is not the case, all facets included in that box are not considered thus relieving the program of a larger computation load. Figure 5 shows the 700X700 m² bounding boxes used in the terrain of study. Terrain sampling interval is 100X100 m², this means that within each bounding box includes 98 terrain facets. Figure 6 further illustrates the bounding box concept.

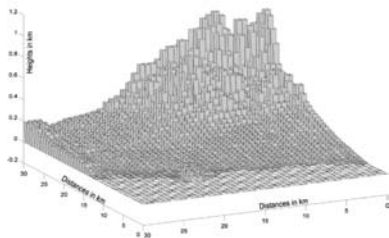


Figure 5. Bounding boxes used in the calculations shown in later sections.

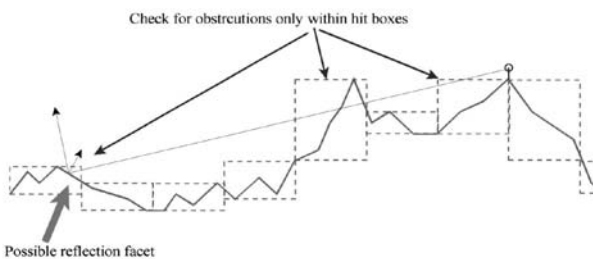


Figure 6. bounding box based acceleration technique.

3. ANTENNA MODELING AND SITTING EFFECTS

UTD techniques have also been used to compute conventional and Doppler VOR antenna patterns and analyze the ground effects for simple 2D terrain and sitting configurations. Figure 7 illustrates the various rays considered for evaluating the radiation pattern of a conventional VOR, CVOR, antenna. The dimensions assumed for the CVOR antenna were: counterpoise diameter, 10 m, Alford loop separations, 0.45 m, and loop height over counterpoise, 1.3 m. The obtained vertical pattern is shown in Figure 8 where gains are given with respect to that of the Alford loop.

Figure 9 shows the various rays considered in the case of the Doppler VOR, DVOR, antenna. The dimensions assumed were: diameter of counterpoise, 30.5 m, radius of ring of Alford loop antennas, 6.25 m and height of antennas above counterpoise, 1.3 m. The obtained vertical pattern is shown in Figure 10 where gains are given with respect to that of the Alford loop.

A number of terrain configurations have been studied for quantifying the influence of the ground on the antenna pattern. Figure 11 shows a schematic diagram where the antenna pattern calculated for free space conditions is set on a linear piece-wise terrain profile and a new radiation diagram is computed now taking into account terrain effects, including its electromagnetic EM constants.

One configuration of particular interest has been that where the VOR antenna sits on a small mesa ending on a cliff-like edge as shown in Figure 12. The distance from the antenna sitting and the mesa's edge was assumed to be 50 m. Figure 13 shows the results for a CVOR and Figure 14 for DVOR both for different counterpoise heights above the ground. Again all gains are referred to that of the Alford loop.

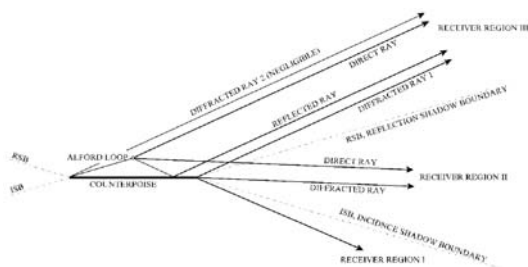


Figure 7. Contributions accounted for in the calculation of the Conventional VOR antenna radiation pattern using UTD.

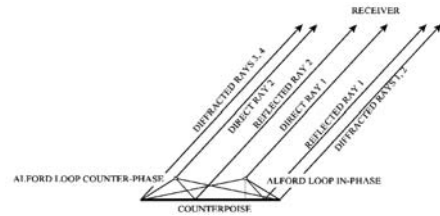


Figure 9. Contributions accounted for in the calculation of the Doppler VOR antenna radiation pattern using UTD.

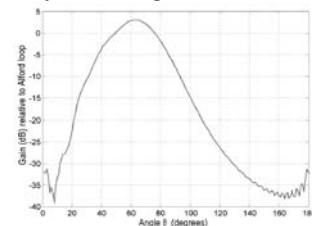


Figure 8. Calculated Conventional VOR antenna radiation pattern using UTD.

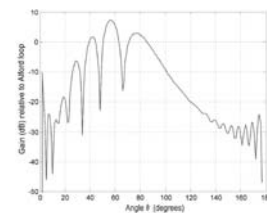


Figure 10. Calculated Doppler VOR antenna radiation pattern using UTD.

The effect of down-sloping terrain has also been studied. Figure 15 illustrates the assumed geometry, where a VOR is sitting on the top of a gently sloping terrain. Figure 16 illustrates the effects on the antenna pattern for a DVOR.

Additionally, the mesa plus cliff configuration has been studied in a different way than above. In this case, the free space antenna pattern is not used first but, rather, the terrain and the various antenna elements are studied together to produce an overall radiation pattern as illustrated in Figure 17 where the rays taken in to consideration are depicted. Figure 18 illustrates the obtained diagram for a DVOR. It can be observed how the results do not differ greatly from the ones shown previously.

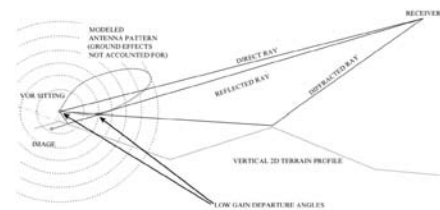


Figure 11. Introducing terrain effects using the antenna pattern computed under ideal free space conditions.

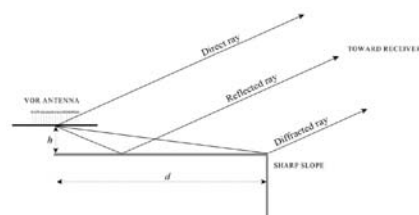


Figure 12. Effect of an antenna sitting at flat area followed by a sharp slope.

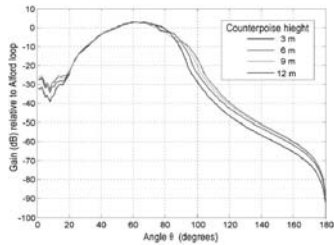


Figure 13. CVOR antenna pattern on a mesa ending on a cliff-like edge

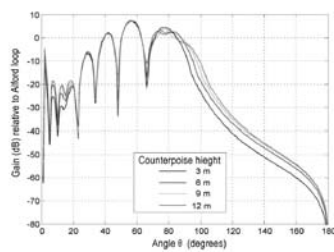


Figure 14. DVOR antenna pattern on a mesa ending on a cliff-like edge.

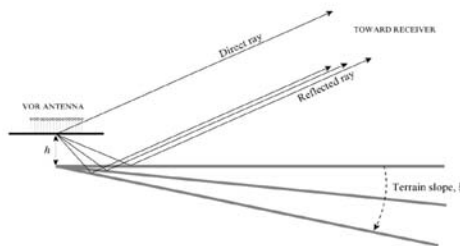


Figure 15. Effect of an antenna sitting at sloping area.

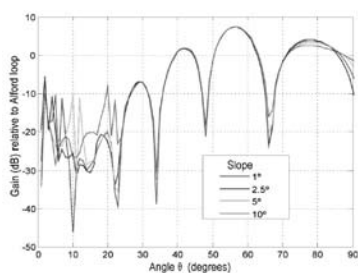


Figure 16. DVOR pattern with sitting on a gently down-sloping terrain. Counterpoise height above the ground, 9 m.

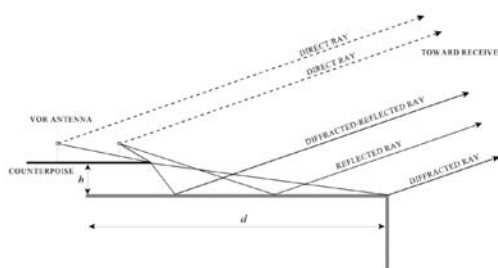


Figure 17. Calculation of terrain effects

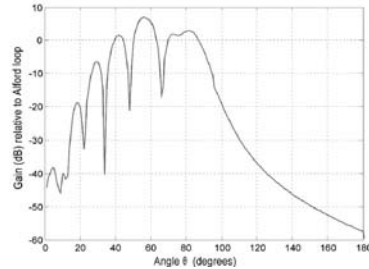


Figure 18. Full UTD analysis on DVOR antenna plus ground (mesa plus cliff).

4. ANALYSIS OF A REAL CASE

The DVOR located near Calella (Spain) near the Mediterranean coast with some higher mountains on the opposite side (see terrain and ray-tracing plots in Figures 19 and 20) has been reported to produce, for some radial flights, very significant bearing errors. In this section propagation data is compared with measured errors for one radial flight. A preliminary study is shown next where only the direct ray and single reflections have been considered. The terrain database used in this study corresponds to 30 km in the E-W and 38 km in the N-S direction. The radial flight followed the S-N direction passing over the VOR. The radial length was approximately 20 nmi and the flight height was 3500 ft.

Figure 21 illustrates the simulated results where traced rays are classified according to their excess delay. At the beginning of the flight strong reflections on the sea surface were found (≈ -5 dB with respect to the direct ray) together with weaker reflections (≈ -13 dB) on the terrain near the VOR. Normally a steady weak reflected ray near the VOR is found for most simulation paths. Also in the plot, the direct signal is shown to have significant lobes for the higher elevation angles, i.e., when the aircraft passes over the VOR as expected from the calculated radiation patterns. The last part of the flight corresponds to non-visibility conditions as the direct radio path is blocked by the mountains behind the VOR station. To accurately model this situation diffracted rays are needed in the study. This has not been implemented yet for the terrain.

Figure 22 shows another plot where the same simulated flight results are presented differently. In this case, the rays traced are classified in terms of the angle of departure from the VOR station. It can be shown how the reflections on the sea depart from the antenna with a very similar angle to that of the direct signal. This leads to very strong reflected rays interfering with the direct signal and producing very large errors.

Figure 23 shows a simulated received electric field time-series (in dBV/m for a normalized transmitted power of 1 W) together with an error time-series for the same test flight. The simulated received signal is not continuous due to the large spacing between samples (100 m). Not considering diffracted or double reflected or mixed rays (e.g., DR) also contributes to the discontinuity of simulated series. However, the spacing used is sufficient for evaluating the carrier over multipath (C/M) parameter as shown in Figure 24 where, if several reflected rays reached the receiver, their power sum was used for calculating the C/M parameter. In this plot, in order to draw a continuous plot, the assumption was made that, for blocked conditions the E field value was -200 dBV/m and, if no reflections existed, the multipath E field was -90 dBV/m. In Figure 25 the results of a more tightly spaced simulation (sampling every 10 m) of the first mile of the test flight are shown. A more continuous time-series is produced in this case. It is clear from this figure, where strong ray interference is apparent, that bearing errors should be quite large as measured.

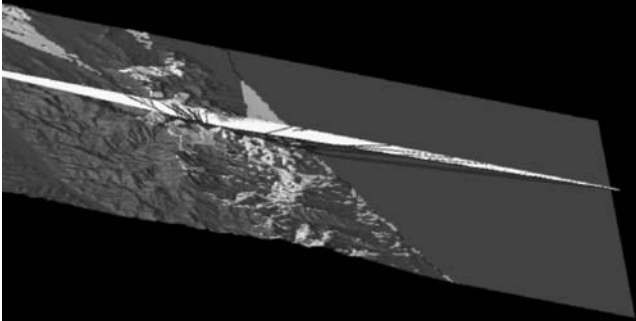


Figure 19. Terrain database, visible areas from DVOR in white and blocked in red. Figure includes ray tracing results for N-S radial flight.

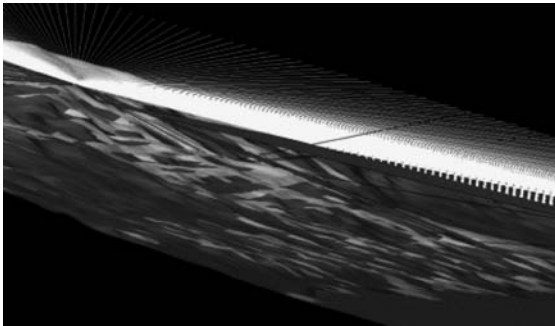


Figure 20. Close-in view of terrain database, visible areas from DVOR in white and blocked in red. Figure includes ray tracing results for N-S radial flight. Yellow lines indicate direct ray and blue lines indicate reflected rays.

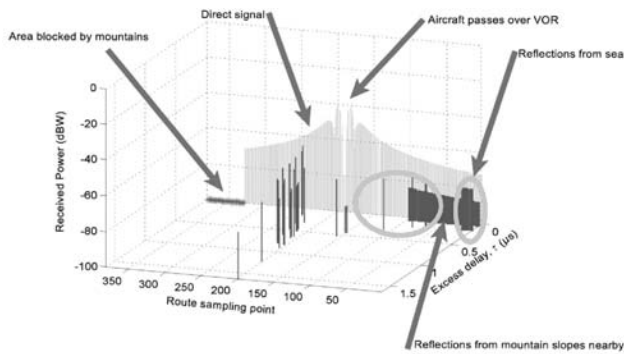


Figure 21. Received rays for a S-N flight passing over the VOR station. Echoes are classified as a function of excess delay relative to the direct ray.

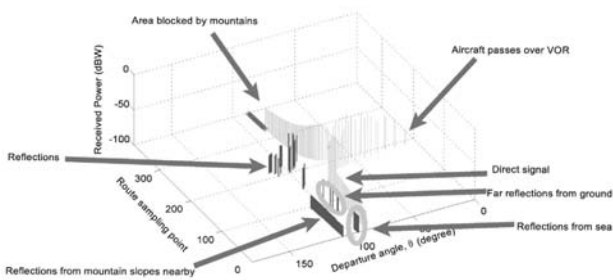


Figure 22. Received rays for a S-N flight passing over the VOR station. Echoes are classified as a function of departure angle.

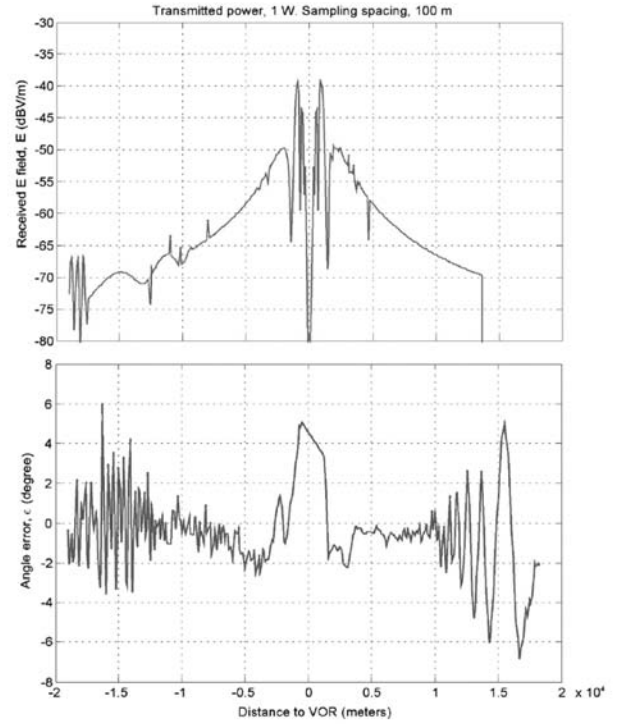


Figure 23. (a) Simulated received field for a S-N flight passing over the VOR station. (b) Measured bearing errors (degree).

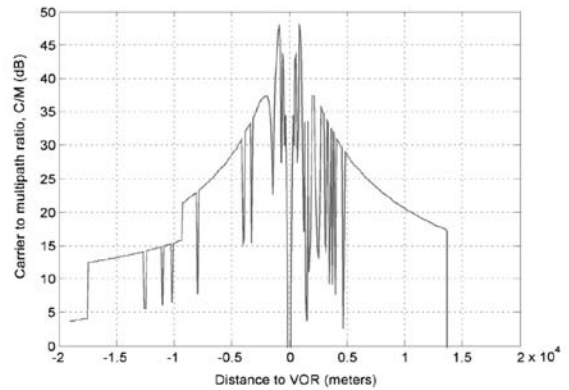


Figure 24. C/M parameter.

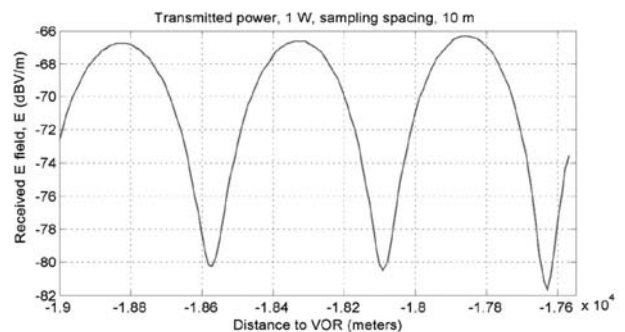


Figure 25. First mile of test flight.

5. SUMMARY AND FUTURE WORK

In this paper a simulation tool for analyzing the influence of terrain irregularity on VOR navigation systems has been presented. This tool is based on ray-tracing techniques and has been developed by the University of Vigo (Spain) for several different scenarios including cellular systems, satellite-to-indoor propagation, the aeronautical channel, etc. Now this tool is being adapted for the analysis of VOR sitting scenarios.

This tool can be used to analyze complex 3D scenarios with terrain databases used as input data. Additionally, vertical 2D profiles can also be studied.

In this paper, also the tool fundamentals have been reviewed and illustration of typical outputs shown. Also, antenna patterns for conventional and Doppler VORs have been presented both under ideal conditions, i.e., in free space and in real conditions for different sitting configurations.

6. REFERENCES

- [1] A.Steingass, A.Lehner, F.P.Fontan, E.Kubista, M.J. Martin and B.Arbesser-Rastburg. The High Resolution Aeronautical Multipath Navigation Channel. ION NTM 2004 Conference, January 26-28, 2004, in San Diego, California USA.
- [2] F.Perez-Fontan, B.Sanmartin, A.Steingass, A. Lehner, E.Kubista and B.Arbesser-Rastburg "Measurements and modeling of the satellite-to-indoor channel for Galileo" ION NTM 2004 Conference, January 26-28, 2004, in San Diego, California USA.
- [3] N.Riera Díaz, B.Sanmartín Pérez and F.Pérez Fontán. Deterministic Propagation Modelling inside Aircraft Cabins. 5th international conference on ITS Telecommunications (ITST 2005) Brest on 27 - 28 - 29 June, 2005 on Telecommunications of Futuristic Transport Environments
- [4] S.R.Saunders. Antennas and Propagation for Wireless Communication Systems. Wiley, 1999.
- [5] G.A.J. Van Dooren . A deterministic Approach to the Modelling of Electromagnetic Wave Propagation in Urban Environments. PhD Thesis. Eindhoven, 1994.
- [6] C.A.Balanis. Advanced engineering electromagnetic. John Wiley, 1989.
- [7] M.F.Cátedra and J.Pérez-Arriaga. Cell planning for wireless communications. Artech House 1999.